Nanoscale Advances

ROYAL SOCIETY OF CHEMISTRY

PAPER

View Article Online
View Journal | View Issue

Cite this: *Nanoscale Adv.*, 2026, **8**, 286

Advanced metal–support interactions in Cu/ZnO catalysts: the role of MOFs and ZrO_2 for enhanced methanol production

Mahdi Pourmand, Ali Haghtalab * and Masoud Safari Yazd *

This study explores the role of metal–support interactions (MSI) and the incorporation of Metal–Organic Frameworks (MOFs) in enhancing the catalytic performance of Cu/ZnO-based catalysts, promoted and supported by Al_2O_3 (ANC) and ZrO_2 (ZNC), for CO_2 hydrogenation to methanol. The ZNC catalyst exhibits significantly superior catalytic performance, achieving up to 90% methanol selectivity and 28% CO_2 conversion under optimal conditions. These improvements are attributed to its higher dispersion, better reducibility, and stronger metal–support interaction (MSI), facilitated by the incorporation of ZrO_2. The use of MOFs in the catalyst synthesis contributes to enhanced stability and active site dispersion. The MSI, coupled with the presence of ZrO_2, facilitates hydrogen spillover, oxygen vacancy formation, and improved CO_2 and H_2 activation. DFT calculations corroborate experimental findings, revealing ZNC's lower activation energy barriers and more efficient pathways for methoxy intermediate formation. This study highlights the critical role of MSI and MOFs in optimizing catalytic efficiency, establishing ZNC as a promising candidate for sustainable methanol production.

Received 31st August 2025
Accepted 17th November 2025

DOI: 10.1039/d5na00838g

rsc.li/nanoscale-advances

1. Introduction

The rapid increase in greenhouse gas emissions, particularly carbon dioxide (CO_2), has led to significant environmental challenges, including global warming and climate change. With atmospheric CO_2 levels rising due to overconsumption of fossil fuels, it is imperative to mitigate emissions and explore sustainable alternatives.[1–3] One promising strategy is the catalytic conversion of CO_2 into valuable chemicals like methanol, which serves as a versatile raw material for fuels and other industrial applications. Methanol synthesis from CO_2 not only reduces greenhouse gas emissions but also enables the recycling of CO_2 into a sustainable "circular carbon economy". This process has the potential to address energy and environmental crises by providing a pathway for renewable fuel production while curbing CO_2 emissions.[4–9] Catalysts play an essential role in the hydrogenation of CO_2 to methanol, enabling the reaction under economically viable conditions. Copper-based catalysts, such as $Cu/ZnO/Al_2O_3$, have long been the industrial standard due to their high activity, stability, and cost-effectiveness.[10]

However, the addition of promoters like transition metal oxides has shown significant improvements in catalytic efficiency by enhancing copper's reducibility, dispersion, and interaction with CO_2. Furthermore, the development of tailored synthesis methods, such as co-precipitation and impregnation, has provided researchers with tools to optimize catalyst performance. These advances allow for the efficient utilization of CO_2 as a feedstock for methanol synthesis, driving progress in sustainable chemical production.[11]

Despite its potential, CO_2 hydrogenation to methanol faces several challenges. The inert nature of the CO_2 molecule requires highly active and selective catalysts to facilitate its transformation under practical reaction conditions.[12] While copper-based catalysts have shown promise, limitations such as sintering, poor stability at lower temperatures, and competing side reactions like reverse water-gas shift (RWGS) need to be addressed. Additionally, achieving a balance between high methanol selectivity and suppressing carbon monoxide formation remains critical. Advanced catalyst designs, including the incorporation of promoters and novel supports, are being explored to overcome these obstacles. Progress in this area holds the key to scalable and efficient CO_2-to-methanol conversion technologies.[1,13–15]

Support materials are crucial in enhancing the performance and longevity of Cu-based catalysts for CO_2 hydrogenation to methanol. These materials stabilize active metal particles, prevent aggregation, and improve the distribution of catalytic sites. Metal oxides like Alumina and carbon-based supports play unique roles: alumina's acidic nature promotes effective dissociation of CO_2, while its high thermal stability ensures structural integrity during reactions.[16] Hierarchical supports, such as MOFs and zeolites, with their micro- and mesoporous structures, ensure efficient reactant accessibility and provide consistent dispersion of Cu nanoparticles.[17,18]

Faculty of Chemical Engineering, Department of Process, Tarbiat Modares University, P.O. Box: 14115-143, Tehran, Iran. E-mail: masoud.safari@modares.ac.ir

Metal–organic frameworks (MOFs), with their crystalline, microporous structures, represent a promising frontier in catalyst development for CO_2 hydrogenation to methanol.[16,19,20] Boasting high surface areas and tunable pore sizes, MOFs such as ZIF-8, composed of Zn^{2+} and 2-methylimidazole, enable precise control over reactant movement, catalyst stability, and performance.[21,22] These frameworks excel in encapsulating Cu nanoparticles (NPs) with high dispersion, leveraging their porosity to minimize particle aggregation and maintain activity over time. The confinement effect within MOFs preserves the Cu catalyst's structural integrity, enhancing metal dispersion and active site exposure critical for efficient CO_2 activation and hydrogenation. By offering these advanced functionalities, MOFs elevate the overall catalytic efficiency and durability, solidifying their importance in sustainable methanol production.[23,24]

Promoters are essential in enhancing the efficiency and performance of Cu-based catalysts for CO_2 hydrogenation to methanol. Metal oxides such as ZnO and ZrO_2 not only act as promoters but also exhibit support characteristics.[25] They can improve electron transfer through their oxygen vacancies, stabilize active sites, and enhance CO_2 adsorption. ZnO plays a crucial role by adsorbing CO_2, facilitating H_2 spillage over Cu, and creating a synergistic system to boost methanol production.[26] However, ZnO's thermal instability and its tendency to promote the reverse water-gas shift (rWGS) reaction at elevated temperatures highlight the need for careful optimization.[27–29]

ZrO_2 plays a multifaceted role in enhancing the performance of Cu/ZnO catalysts for CO_2 hydrogenation to methanol. It acts as a co-support that significantly improves Cu and ZnO dispersion, enhances redox properties, and strengthens metal–support interactions. These properties contribute to higher catalytic activity and methanol selectivity, particularly at low reaction temperatures (150–240 °C). The weak hydrophilic nature of ZrO_2 also facilitates water desorption, thermodynamically promoting methanol synthesis. In addition, the unique amphoteric properties of ZrO_2, combining weak acidic and basic characteristics, allow it to interact effectively with CO_2 and CO, stabilizing intermediates and aiding in their transformation into methanol. Its ability to form amorphous structures or interact with crystalline Cu/ZnO enhances the adsorption and activation of CO_2, while optimizing the dissociative adsorption of intermediates like formate. Furthermore, the particle size and crystallinity of ZrO_2 strongly influence its synergy with Cu and ZnO, with smaller or amorphous ZrO_2 structures demonstrating enhanced methanol yield by creating highly active sites. ZrO_2's versatility extends to its role in oxide–oxide interactions, such as forming ZrO_2–ZnO interfaces, which boost CO_2 conversion efficiency and methanol selectivity. These interfaces optimize adsorption properties, stabilize active intermediates, and enhance catalytic stability under reaction conditions. Its tunable physicochemical properties, such as surface acidity, basicity, and oxygen vacancy concentration, make ZrO_2 a critical component in advancing the design of next-generation catalysts for sustainable methanol production from CO_2 hydrogenation.[30–32]

In this study, to achieve an efficient catalyst for CO_2 hydrogenation to methanol, we employ ZIF-8 as a superior support for Cu NPs, which are interconnected with Zn NPs through a thin porous carbon interface derived during the catalyst fabrication process. To further enhance catalyst stability and improve its catalytic performance, additional metal oxides, ZrO_2 and Al_2O_3, are employed as supports and promoters. Although these metal oxides have been extensively studied, their specific role in metal–support interaction (MSI) in Cu-based catalyst has not been thoroughly investigated. This study not only evaluates their characteristics using various analytical techniques and examines their catalytic performance comprehensively but also compares their features theoretically through density functional theory (DFT). Unique attributes, such as their role in hydrogen spillover and their influence on strengthening the MSI, are analyzed, highlighting their importance in methoxy formation, a key intermediate in the methanol production process.

2. Experimental method

2.1 Catalyst synthesis

The catalyst fabrication is conducted through a multi-step process. First, the synthesis of the zeolitic imidazolate framework (ZIF-8) is performed using $Zn(MeIm)_2$ (where MeIm stands for 2-methyl imidazolate). At this stage, the active site incorporates both Zn and Cu metals, requiring the simultaneous addition of $Cu(NO_3)_2\cdot 3H_2O$ and $Zn(NO_3)_2\cdot 6H_2O$ in a 2 : 1 molar ratio to the 2-methyl imidazolate solution.[21] Next, the Cu-doped ZIF-8 structure is encapsulated with zirconia using a deposition precipitation method, followed by thermal treatment. Initially, pyrolysis is carried out at 450 °C for 3 hours under a nitrogen atmosphere to convert the ZIF-8 structure into a porous carbon framework. This is followed by calcination at 350 °C for 5 hours, which results in the formation of a thin porous carbon layer. As highlighted by Wang *et al.*, the combined effects of pyrolysis and calcination improve the reducibility, dispersion, and crystal size reduction of particles.[22] While calcination in air can partially remove the carbon layer, the chosen calcination conditions ensure that complete carbon removal does not occur.[33] After the thermal treatment, the resulting catalyst appears as a blackish-brown powder. For comparison, a conventional Al_2O_3 promoter–support was applied to prepare the catalyst using a similar MOF-structure-assisted method, aiming to achieve a catalyst with a suitable narrow mesopore size distribution and an enlarged interfacial area at the metal-oxide interface. The detailed synthesis procedures will be discussed in the subsequent sections.

2.1.1 Catalyst preparation

2.1.1.1 Synthesis of Cu-doped ZIF-8. Typically, 5 g of $Cu(NO_3)_2\cdot 3H_2O$, 3 g of $Zn(NO_3)_2\cdot 6H_2O$, and 0.3 g of CTAB were dissolved in 60 mL of methanol to prepare solution 1, and the mixture was stirred for one hour. Separately, 12 g of 2-methylimidazole was dissolved in 60 mL of methanol to prepare solution 2. Solution 1 was then slowly added to solution 2 while stirring, and the combined mixture was stirred at room temperature for 2 hours. After this stage, the solution was left

undisturbed for 24 hours to allow the crystallization of ZIF-8. To obtain Cu-doped ZIF-8, the resulting moist sample was dried in a vacuum oven at 90 °C for 12 hours.

2.1.1.2 Synthesis of CuO@ZnO/ZrO_2 (ZNC). In this step, 4 g of Cu-doped ZIF-8 were dispersed in 50 mL of ethanol. Separately, 1 g of $Zr(NO_3)_2 \cdot 6H_2O$ was dissolved in 50 mL of water. These two solutions were gently mixed, and ammonium carbonate was added to precipitate zirconium as zirconium carbonate. The mixture was stirred for 9 hours at 60 °C to remove excess moisture and subsequently dried at 90 °C for 12 hours in a vacuum oven. The resulting product was then subjected to the specified thermal treatment program to produce the final CuO@ZnO/ZrO_2 (ZNC).

2.1.1.3 Synthesis of CuO@ZnO/Al_2O_3 (ANC). Similar to the ZNC synthesis, 4 g of Cu-doped ZIF-8 were dispersed in 50 mL of ethanol. Subsequently, 1.5 g of $Al(NO_3)_3 \cdot 9H_2O$ was dissolved in another 50 mL of water. These two solutions were then gently mixed. Afterward, ammonium carbonate was added to precipitate $Al_2(CO_3)_3$, and the mixture was subjected to the same thermal treatment used for ZNC to achieve the final CuO@ZnO/Al_2O_3 (ANC).

2.2 Characterization method

For the structural characterization of the catalyst, a range of analyses is necessary, such as X-ray diffraction (XRD). The XRD patterns are obtained using a Philips X'Pert MPD X-ray diffractometer with monochromatic Cu-Ka radiation ($\lambda = 0.179026$ nm). Additionally, eqn (1), known as the Scherrer equation, is used to examine the size of the crystalline particles, where λ represents the wavelength value β denotes the peak width at half its maximum height and K is the shape factor, typically about 0.9.

$$D = \frac{K\lambda}{\beta \cos\theta} \quad (1)$$

The BET(Brunauer–Emmett–Teller) surface area and pore volume of the samples were determined using the nitrogen adsorption/desorption method with a Micromeritics Tristar 3020 analyzer on the sample was degassed.[34] The TESCAN MIRA3 helps us map out the elemental composition using FE-SEM/EDS. The reducibility of catalyst samples and temperature-programmed analyses, including H_2-TPD, oxygen titration, and TPR, were investigated using a U-tube quartz reactor equipped with a Quantachrome CHEMBET-3000 unit featuring a thermal conductivity detector (TCD). For TPR, a 10 vol% H_2/Ar flow (30 mL min^{-1}) was used, with the temperature ramped at 5 °C min^{-1} from room temperature to 900 °C. Metal dispersion was determined from H_2 uptake during TPD, calibrated with gas standards and accounting for catalyst-specific parameters such as weight, stoichiometry, and metal loading. Active copper metal particle size was estimated assuming spherical crystallites, based on the relationship between surface area, density, and dispersion. The degree of catalyst reduction (DOCR%) was measured *via* O_2 titration, re-oxidizing the reduced catalyst and quantifying oxygen uptake, with calculations based on the stoichiometry of copper oxidation (Cu^0 to CuO). For CO_2/H_2-TPD, 0.05 g of reduced sample was exposed to CO_2/H_2 at 40 °C for 1 hour, purged with He for 30 minutes to remove physically adsorbed species, and subsequently analyzed by TPD with a temperature ramp of 10 °C min^{-1} up to 1000 °C in a helium stream (20 mL min^{-1}).[33,35]

2.3 Performance test

The catalyst performance in the CO_2 hydrogenation process is assessed using a mini vertical fixed-bed reactor with a 10 mm inner tube diameter. To ensure even heat distribution, 0.3 g of each catalyst is loaded into the reactor along with silicon carbide, filling the reactor. The reactor's temperature is gradually increased at a rate of 1 °C per minute from room temperature to 475 °C and maintained at this level for 12 hours under hydrogen flow to activate the catalyst by reducing it. After cooling the reactor to operating conditions and reaching a steady state, CO_2 hydrogenation reaction experiments are conducted. Digital mass flow controllers and pressure regulators manage the feed gas flow rate and pressure. The setup, depicted in Fig. 1, includes a mini tubular fixed-bed reactor, mass flow controllers (MFCs), and a temperature controller (TC). Operating conditions for CO_2 hydrogenation include a constant temperature of 150 °C, a feed ratio of $H_2/CO_2 = 3/1$, and a GHSV of 4000 h^{-1}, with varying pressure values of 25, 27.5, and 30 bar, respectively.[36–39]

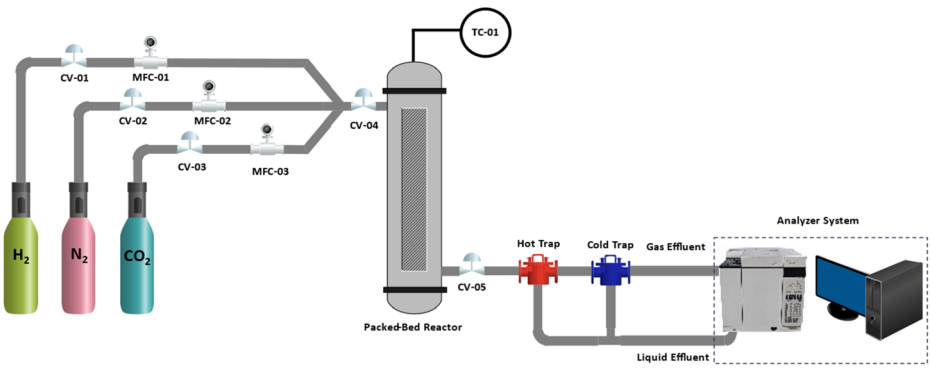

Fig. 1 Fixed bed catalytic performance setup.

After the process is completed in the reactor, the product is analyzed using a GC analysis system (Agilent 7890A). By examining both the gas and liquid phases in the analyzer, CO_2 conversion, methanol selectivity (S_M), and the productivity of methanol (P_M) can be determined using eqn (2)–(4).

$$X_{CO_2} = \frac{F_{CO_2in} - F_{CO_2out}}{F_{CO_2in}} \quad (2)$$

$$S_M = \frac{F_M}{F_{CO_2in} - F_{CO_2out}} \quad (3)$$

$$P_M = \frac{\text{mole of methanol}}{W_{cat} \times t} \quad (4)$$

where F_{CO_2}, F_M, W_{cat}, and t denote the molar fraction of CO_2, methanol, weight of the catalyst (kg), and time (h), respectively.

2.4 Technical description of molecular simulation

Density Functional Theory (DFT) is a robust computational technique widely employed to explore molecular interactions and perform simulations across various domains of materials analysis. It leverages quantum mechanical principles to investigate and predict atomic-scale interactions with high accuracy. In this study, the DFT calculations were carried out using the Abinit software package,[21,40] while the initial atomic structures were designed with the Avogadro and Packmol tools.[22,33,41,42] A magnified visualization of the designed structures is presented in Fig. 2, with graphical outputs generated using the OVITO software,[34] which enables clear and detailed analysis of the atomic configurations.

Following the structural design phase, the atomic models were subjected to full optimization using the Broyden–Fletcher–Goldfarb–Shanno (BFGS) minimization algorithm. This procedure continued iteratively until the residual forces acting on each atom converged to a constant value below 0.001 hartree per Å, ensuring precise structural stability.[35]

Technically, the wave functions were represented using a plane-wave basis set with an energy cut-off value of 300 hartree, applied consistently to all atomic models. For reciprocal space calculations, the Monkhorst–Pack method was utilized to generate an optimized 8 × 8 × 8 k-point mesh within the Brillouin zone.[43] In these interaction simulations, valence electrons were explicitly considered, while the influence of core electrons was accounted for using pseudo-potentials derived from the Projector Augmented Wave (PAW) methodology. The atomic species included in the calculations, namely Cu, Zn, O, Al, and Zr, were modeled with high fidelity using this approach.[44–47]

To achieve reliable and accurate electronic structure calculations, the Generalized Gradient Approximation (GGA) was implemented with the Perdew–Burke–Ernzerhof (PBE) functional for exchange–correlation approximations.[19,48] Additionally, the self-consistent field (SCF) iteration process was performed with a strict convergence threshold set to 10^{-30} hartree, ensuring a high degree of precision in the energy calculations.

3. Result and discussion

3.1 Characterization

The XRD profiles of the two catalysts (Fig. 3), ANC and ZNC, provide significant insights into their structural and textural properties. For both catalysts, characteristic diffraction peaks of CuO are observed at 2θ values of 35.6° and 38.9°, corresponding to the (002) and (111) planes of copper oxide crystals, respectively, which align well with the standard JCPDS 05-0661.[49]

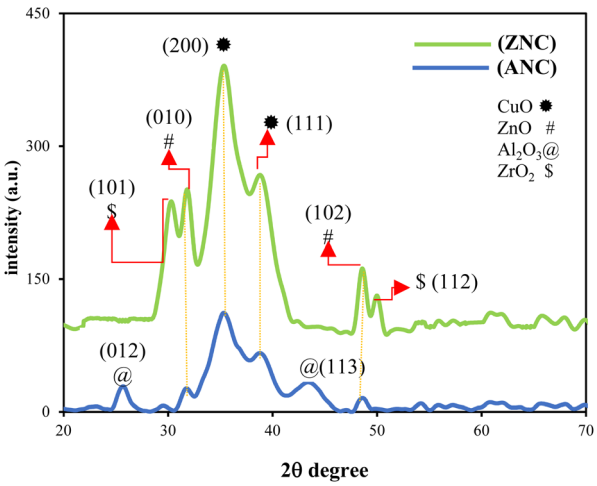

Fig. 3 X-ray diffraction patterns of ANC and ZNC catalysts.

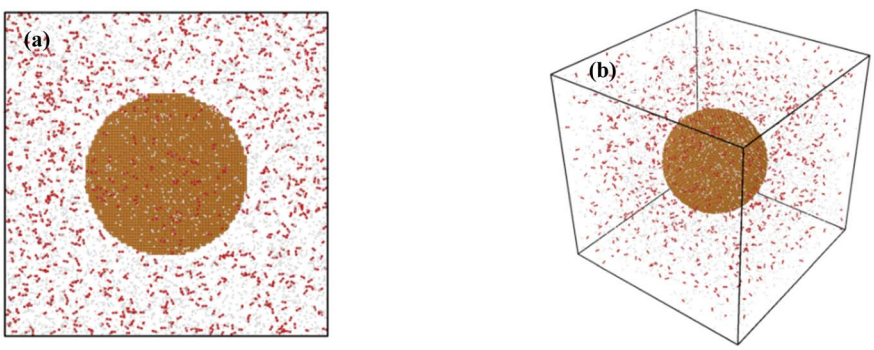

Fig. 2 (a) Zoomed-in snapshot of a designed atomic sample; (b) perspective view of the geometry-optimized atomic structure.

Additionally, peaks at 31.8° and 48.6° indicate the presence of ZnO crystalline phases, attributed to the (010) and (102) planes, as per the standard JCPDS 900-8878.[43,44] However, the ZNC catalyst exhibits significantly higher peak intensity compared to ANC, highlighting zirconia's role in enhancing crystallinity and stabilizing the catalyst structure.

The unique contribution of ZrO_2 in the ZNC catalyst is further validated by the presence of additional peaks at 30.27° and 50.26°, corresponding to the (101) and (112) planes of zirconia, which align with the standard JCPDS 210-0389.[50] This contrasts with ANC, which lacks these peaks but instead shows weak reflections at 25.57° and 43.39°, attributed to alumina crystals (planes (012) and (113)) based on JCPDS 46-1212.[19,48]

These observations emphasize the MSI distinctions between the two catalysts, with ZNC demonstrating greater crystalline order and more uniform dispersion of active components (Table 1). The smaller Cu particle size in ZNC, as indicated by the XRD analysis ($D^a = 8.0 \pm 0.1$ nm), contrasts with the slightly larger particle size in ANC ($D^a = 9.1 \pm 0.1$ nm).

Although, as Murthy *et al.*[16] noted, Cu particle sizes in both catalysts fall within the optimal size range (>8 nm), which is crucial for minimizing side reactions, the smaller size in ZNC provides a distinct advantage. The enhanced catalytic activity in CO_2 hydrogenation to methanol can be attributed to the smaller Cu particle size, which increases active site availability and facilitates sufficient charge transfer for adsorbing intermediate species.[16] This structural feature of ZNC positions it as the more active catalyst for methanol synthesis.

The observed differences in the XRD profiles and particle sizes can be attributed to the distinct roles of ZrO_2 and Al_2O_3 as supports and promoters in the catalyst matrix. Zirconia, evident in ZNC, significantly enhances crystallinity and provides a stable framework for Cu and ZnO dispersion through the porous carbon structure derived from ZIF-8. This highlights the importance of strong metal–support interactions facilitated by ZrO_2. These interactions can improve the activation of CO_2 and hydrogen, boosting methanol yield while suppressing side reactions like the reverse water-gas shift (rWGS).

In contrast, the alumina support in ANC contributes to larger Cu particle sizes (9.1 nm), which correlate with a reduced surface area and fewer active sites. These differences impact catalytic performance, with ANC exhibiting slightly diminished CO_2 adsorption and stabilization of intermediate species. Furthermore, the weaker crystalline order observed in ANC suggests less efficient metal–support interactions, which may reduce the overall activity of the catalyst in CO_2 hydrogenation.

Table 1 The textural characteristics of all catalysts, the average size of catalyst particles was measured (D^a from XRD and D^b from H_2-TPD/O_2 titration). The distribution of Cu particles and their dispersion were assessed through H_2-TPD and oxygen titration

Catalyst	D^a (nm)	D^b (nm)	DOR%	Dispersion %
ZNC	8.0 ± 0.1	9.2 ± 0.5	84.2	12.5
ANC	9.1 ± 0.1	10.1 ± 0.5	72.2	9.5

The structural and textural properties, as influenced by the support–promoter combination, play a pivotal role in optimizing catalyst performance for methanol synthesis. ZNC's attributes make it a more promising candidate for industrial applications requiring high activity and selectivity.

The N_2 adsorption–desorption isotherm and pore size distribution results are shown in Fig. 4 which reveal important insights into the structural differences and surface properties of the ANC and ZNC catalysts. Both catalysts exhibit Type IV adsorption isotherms, which are indicative of mesoporous materials. However, the nature of the hysteresis loops differs significantly. ZNC displays an H3 hysteresis loop within the relative pressure range of 0.75. These features suggest the presence of a narrow pore size distribution with open ends, enhancing accessibility for reactant molecules. In contrast, ANC exhibits an H1 hysteresis loop within the relative pressure range of 0.58, signifying a more uniform mesoporous structure (Table 2).[20,51]

The BET surface area (S_{BET}) values further emphasize the structural differences. ZNC demonstrates a higher surface area of 135 $m^2\ g^{-1}$ compared to 106 $m^2\ g^{-1}$ for ANC. The larger surface area of ZNC correlates with its adequate MSI values, which reduce metal site agglomeration, facilitate greater dispersion of Cu/ZnO particles, and will enhance the accessibility of active sites. The total pore volume (V_p) of ZNC, at 0.2 $cm^3\ g^{-1}$, is marginally higher than that of ANC, which is 0.19 $cm^3\ g^{-1}$. Additionally, the pore diameter (P_D) is slightly smaller for ZNC (5.1 nm) compared to ANC (5.4 nm), indicating tighter pore structures in ZNC. These values represent the primary pore diameters derived from BET surface area analysis, and while the measured pore diameters are slightly smaller than the particle sizes (8 nm for ZNC and 9 nm for ANC), the difference is likely

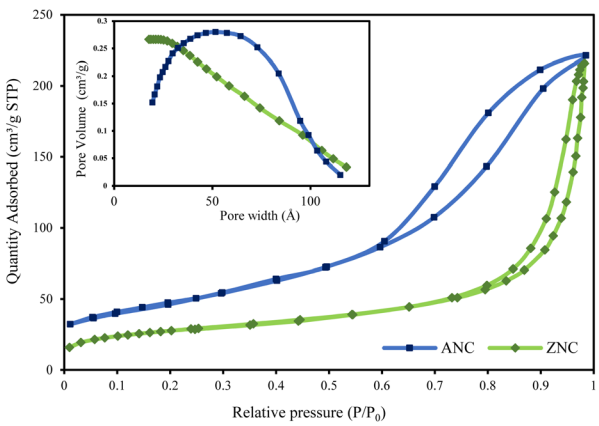

Fig. 4 N_2-physisorption isotherms and pore size distributions of the catalysts.

Table 2 The physicochemical properties of catalysts were determined using N_2 adsorption isotherms

Catalyst	S_{BET} ($m^2\ g^{-1}$)	V_p ($cm^3\ g^{-1}$)	P_D (nm)
ZNC	135	0.2	5.1
ANC	106	0.19	5.4

due to secondary contributions from interstitial voids between the particles. The reported pore diameters are primarily attributed to the mesoporous structures within the materials, with interstitial voids potentially influencing the overall porosity but not constituting the primary source of the measured pore diameter. This structure not only enhances surface area but also improves mass transfer and dispersion of active sites, which are critical for catalytic activity in CO_2 hydrogenation. The narrow pore size in ZNC promotes effective diffusion of reactants and intermediates, leading to improved catalytic performance.

Conversely, the ANC catalyst has a relatively uniform mesoporous structure but lacks the benefits of high surface area. Al_2O_3 contributes to a stable framework but does not facilitate the same level of surface area, optimized pore structure as ZrO_2. These structural advantages make ZNC a more promising candidate for industrial applications, particularly in processes requiring high catalytic efficiency and stability.

FESEM/EDS analysis was utilized to investigate the surface characteristics and structural morphology of the synthesized catalysts, with particular attention to the effective preservation of the carbon coating through controlled calcination processes.[22] This detailed analysis provided insights into the compositional variations, as presented in Table 3. The FESEM/EDS results (Fig. 5) highlighted significant differences in the structural and elemental distribution of the ZNC and ANC catalysts, underscoring the roles of ZrO_2 and Al_2O_3 as supports–promoters in CO_2 hydrogenation to methanol. Notably, both catalysts exhibited roughly similar elemental proportions. Additionally, the carbon and nitrogen contents, attributable to the nitrogen-doped porous carbon layer derived from the ZIF-8 precursor, play a crucial role. This nitrogen-functionalized carbon layer is instrumental in enhancing the dispersion of Cu/ZnO particles, stabilizing active sites, and strengthening metal–support interactions (SMSI). This is consistent with findings by Wang *et al.*,[52] where nitrogen-functionalized carbon nanotubes (N-CNTs) improved Cu oxide dispersion, reducibility, and H_2/CO_2 adsorption capacity, thereby boosting methanol synthesis activity. The nitrogen-doped carbon in these catalysts likely plays a similar role, increasing H_2 dissociation and CO_2 adsorption, which strengthen the catalyst's overall performance.

Furthermore, the particle size distribution diagram of each catalyst, as shown in Fig. 5, reveals that ZNC exhibits an average particle size of 14.9 nm, with smaller and more uniformly distributed particles encapsulated within a matrix. This structure promotes improved Cu–ZnO dispersion and enhances catalytic stability. In contrast, ANC displays a larger average particle size of 16.5 nm with irregularly distributed particles, indicative of weaker metal–support interactions and reduced stability.

Table 3 Elemental content and particle average size of both catalysts using FE-SEM/EDX

Catalyst	Elemental content (wt%)							Particle average size (nm)
	Cu	Zn	C	N	O	Al	Zr	
ZNC	39.13	19.15	7.29	1.61	24.71	—	8.11	14.9
ANC	39.24	19.06	7.33	1.59	24.61	8.17	—	16.5

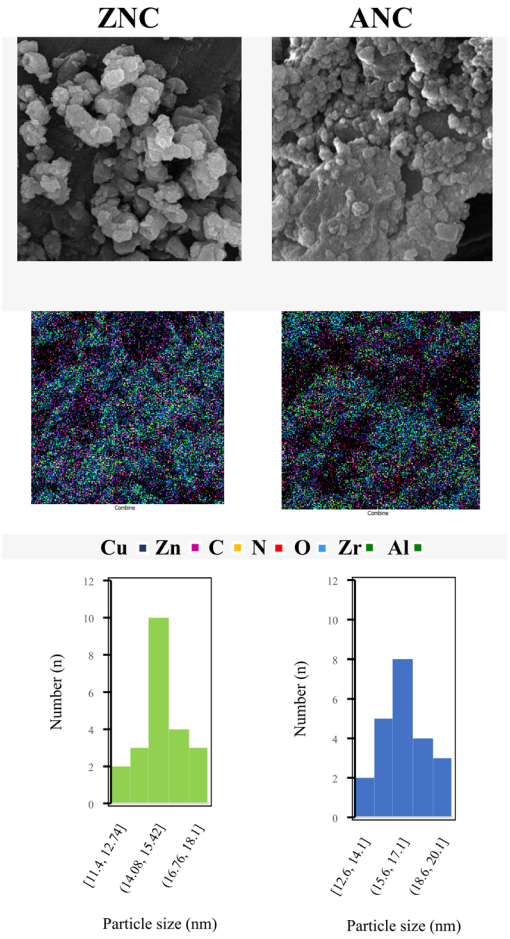

Fig. 5 Images, elemental and particle size distribution of all catalysts by FESEM/EDS mapping.

The H_2-TPR profiles of the ANC and ZNC catalysts which are exhibited on Fig. 6 present significant differences in their

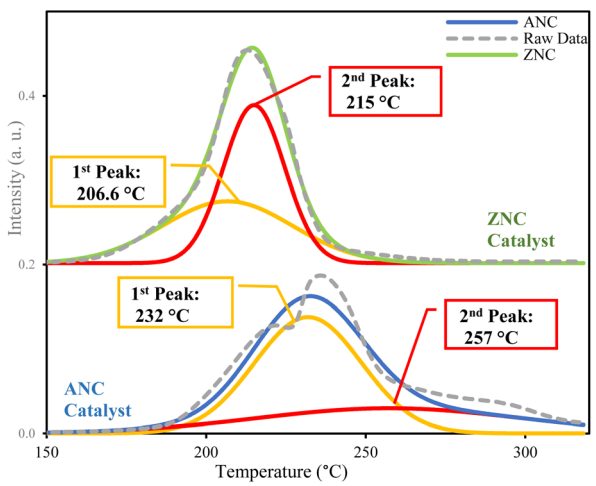

Fig. 6 H_2-TPR profiles of both catalysts.

reduction behaviors, primarily due to the nature of their respective supports and promoter structures. For both catalysts, the profiles were deconvoluted into two main peaks, corresponding to the reduction stages of CuO to Cu^{+} and Cu^{+} to Cu^{0}.[53,54] In the ZNC catalyst, the first reduction peak occurs at a lower temperature (206.6 °C) compared to ANC (232 °C), reflecting the reduction of highly dispersed CuO clusters or isolated Cu^{2+} ions. Similarly, the second peak in ZNC appears at 215 °C, while in ANC it is shifted to 257 °C. These shifts indicate that the ZNC catalyst exhibits easier and more efficient reducibility of copper oxide species compared to ANC.

The enhanced reducibility of the ZNC catalyst can be attributed to the synergistic effects of the ZrO_2 promoter, which facilitates oxygen vacancy formation and hydrogen spillover. Zirconia, in its reduced Zr^{3+} state, serves as an active site for oxygen vacancy formation and interacts with copper oxide species, significantly lowering their reduction energy barrier. This interaction not only enhances the activation of CuO species but also improves the catalyst's reducibility. The fine-tuning capability of the Cu–ZrO_2 interface stabilizes Cu cations, which act as electron acceptors during catalytic processes, thereby boosting methanol production selectivity and activity.[55–57]

These features create an optimized environment for improved reducibility and stabilization of key intermediates essential for catalytic efficiency. In contrast, the ANC catalyst, supported by Al_2O_3, exhibits higher reduction temperatures due to larger copper oxide particles, as confirmed by XRD analysis, and the absence of oxygen vacancy formation capability in Al_2O_3. This limitation leads to a less effective reduction environment for CuO species and reduced catalytic efficiency in CO_2 hydrogenation to methanol.

On the other hand, the comparison of ZNC and ANC catalysts through H_2-TPD/O_2 titration reveals key differences in their textural and functional properties, as illustrated in Table 1. The average particle size derived from H_2-TPD/O_2 titration (D^b) highlights that ZNC exhibits smaller particle sizes (9.18 nm) compared to ANC (10.14 nm). The smaller particle size of ZNC indicates better dispersion of active copper species, which is confirmed by its higher dispersion percentage of 12.46%, compared to 9.52% for ANC.

The degree of reducibility (DOR%) is another critical parameter, where ZNC achieves a higher value (84.21%) than ANC (72.23%). This improved reducibility of ZNC is attributed to the synergistic effects of ZrO_2 as a promoter. The zirconium oxide promotes hydrogen spillover and enhances the reducibility of copper oxide species. In contrast, the ANC catalyst, supported by Al_2O_3, presents larger copper oxide particles and reduced dispersion, which may result in weaker performance in spillover phenomena.[58]

The superior reducibility of the ZNC catalyst is attributed to its unique structural and chemical properties. Encapsulation of Cu/ZnO particles within a porous carbon layer derived from ZIF-8 ensures improved particle dispersion and accessibility of active sites. In contrast, the ANC catalyst, supported by Al_2O_3, exhibits larger copper oxide particles, as confirmed by XRD analysis. Al_2O_3 lacks the reducibility and fine-tuning capabilities of ZrO_2, leading to weaker interactions with Cu species and limiting the reduction process. This results in reduced dispersion of active copper sites and can negatively impact overall catalytic performance. The higher DOR% of ZNC compared to ANC aligns with the TPR analysis, indicating lower reduction temperatures for ZNC and better activation of CuO species. This enhanced activation contributes to superior hydrogenation activity and methanol selectivity. Additionally, ZNC's higher dispersion percentage, consistent with the literature, highlights the role of ZrO_2 in improving metal–support interactions and stabilizing active sites.

Furthermore, the H_2-TPD results, which are depicted in Fig. 7a, highlight the distinct hydrogen adsorption and spillover behaviors of the ZNC and ANC catalysts, revealing the influence of the ZrO_2 and Al_2O_3 supports on their performance. The ZNC

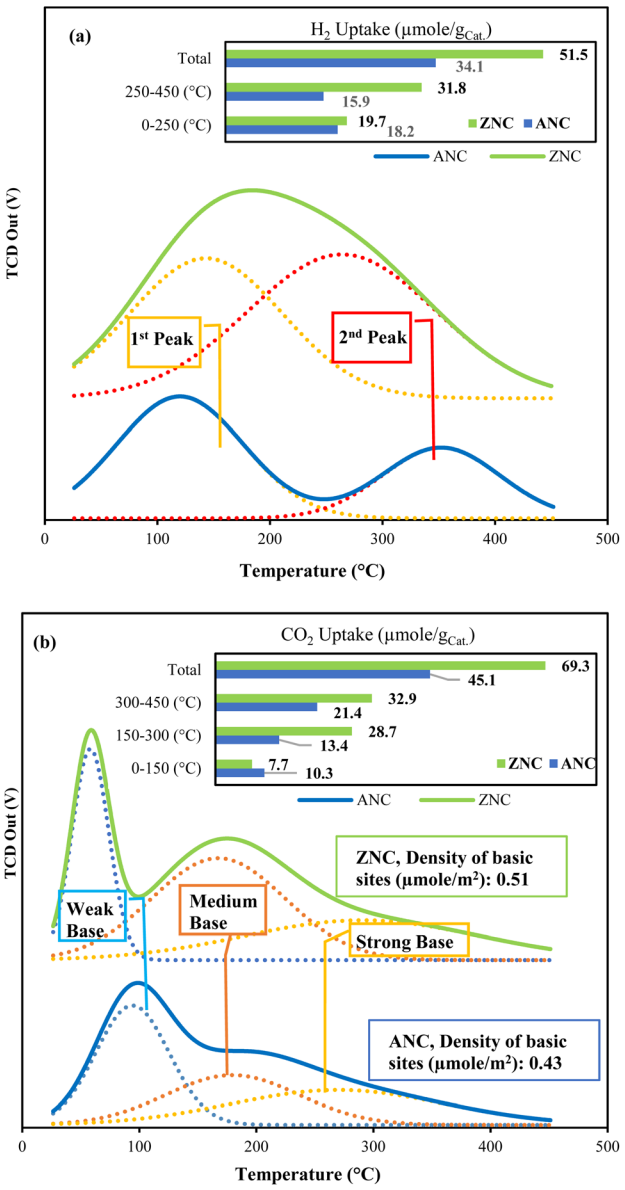

Fig. 7 (a) H_2-TPD and (b) CO_2-TPD profiles: comparative analysis of basicity and hydrogen uptake in ZNC and ANC catalysts.

catalyst demonstrated a superior H_2 uptake value in both the low-temperature range (19.7 μmol g_{cat}^{-1}) and the high-temperature range (31.8 μmol g_{cat}^{-1}) compared to the ANC catalyst, which exhibited H_2 uptake values of 13.5 μmol g_{cat}^{-1} and 15.9 μmol g_{cat}^{-1}, respectively. This indicates that the ZNC catalyst is more effective in both hydrogen chemisorption and facilitating spillover, key factors for catalytic activity in CO_2 hydrogenation to methanol.[59,60]

The enhanced hydrogen uptake and spillover behavior of the ZNC catalyst are strongly influenced by the properties of ZrO_2, which acts as a superior support–promoter. ZrO_2 enhances hydrogen spillover through its ability to create oxygen vacancies and interact with hydrogen *via* Kubas-type interactions.[50,61,62] These interactions involve electron transfer and back donation between the Zr 3d orbital and the hydrogen 1s orbital, improving both adsorption and spillover processes. Additionally, the ZNC catalyst's structure, with Cu/ZnO particles encapsulated in a porous carbon layer derived from ZIF-8, enhances the dispersion and accessibility of active sites. This synergy between ZrO_2's electronic properties and the optimized structural characteristics facilitates a highly efficient activation of hydrogen, crucial for CO_2 hydrogenation to methanol.

In contrast, the ANC catalyst, supported by Al_2O_3, demonstrates significantly weaker metal–support interactions (MSI). Unlike ZrO_2, Al_2O_3 lacks the electronic properties and tunable oxygen vacancy concentrations necessary to effectively promote hydrogen spillover. This limitation results in lower hydrogen uptake and reduced spillover efficiency, as observed in the H_2-TPD results. Consequently, the weaker MSI in ANC leads to diminished stabilization and activation of active sites, negatively impacting its overall catalytic performance.

The contrast in hydrogen spillover behaviors highlights the pivotal role of MSI in shaping catalytic outcomes.[58] In the ZNC catalyst, the enhanced MSI facilitated by ZrO_2 not only improves hydrogen chemisorption but also stabilizes reactive intermediates, enabling better hydrogen mobility and surface coverage. These factors collectively contribute to ZNC's superior catalytic efficiency for CO_2 hydrogenation to methanol. The integration of ZrO_2 underscores the strategic importance of support–promoter selection in optimizing MSI, hydrogen spillover, and overall catalytic performance.

The CO_2-TPD results reveal significant differences in the basicity and CO_2 adsorption capabilities of the ZNC and ANC catalysts. The ANC catalyst exhibits a higher CO_2 uptake at lower temperatures (0–150 °C), indicating a greater presence of weak basic sites attributed to surface hydroxyl groups. Conversely, the ZNC catalyst shows superior CO_2 uptake at medium (150–300 °C) and strong (300–450 °C) basic sites, corresponding to oxide pairs and unsaturated oxygen ions (O^{2-}), respectively. These strong basic sites are closely linked to methanol synthesis, as they correlate with the active sites for CO_2 hydrogenation.[63]

The enhanced basicity of ZNC is attributed to the zirconia support, which facilitates the formation of oxygen vacancies and contributes to stronger adsorption sites. ZNC also demonstrates a higher density of total basic sites (0.51 μmol m^{-2}) compared to ANC (0.43 μmol m^{-2}), emphasizing the dual contribution of its surface area and basic strength. This superior basic site density likely enhances the catalyst's performance by providing more active sites for CO_2 activation and conversion.

In comparison, the ANC catalyst, supported by Al_2O_3, lacks the ability to create robust adsorption sites due to the inert nature of Al_2O_3 in facilitating oxygen vacancy formation. The weaker interaction between Cu species and Al_2O_3 results in a lower overall basicity and a reduced ability to adsorb and activate CO_2, which can limit its catalytic efficiency in methanol production.

The disparities in CO_2 uptake and basic site distribution between ZNC and ANC catalysts are rooted in the differing properties of their supports. ZrO_2 in the ZNC catalyst enhances the formation of medium and strong basic sites, which are critical for methanol synthesis. The presence of a porous carbon

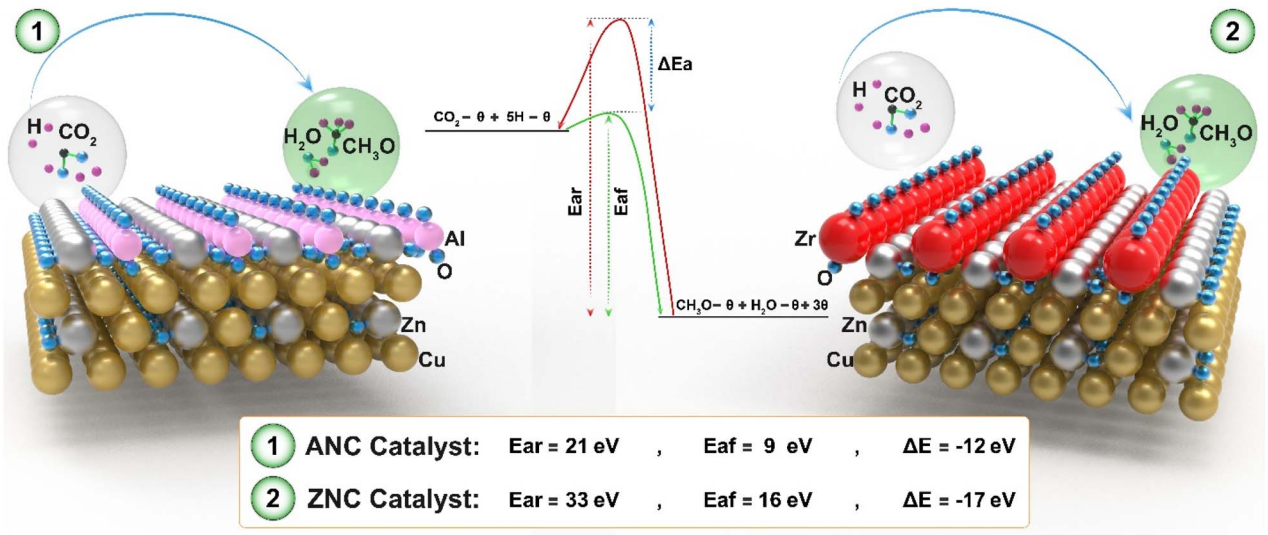

Fig. 8 The forward and reverse energy barriers for the methoxy formation reaction on both catalysts were calculated using DFT.

layer further increases the accessibility of these sites, providing a synergistic effect. Al_2O_3, on the other hand, lacks this capability, resulting in fewer strong basic sites and diminished catalytic activity. Thus, the structural and compositional advantages of ZNC underline its superior performance in CO_2 hydrogenation to methanol. Future research could explore further optimization of zirconia-based systems to enhance basicity and catalytic efficiency.

3.2 Molecular computation

The DFT results which are depicted in Fig. 8 and presented in Table 4 provide a comprehensive distinction between the ZNC and ANC catalysts, emphasizing the critical influence of their respective supports—ZrO_2 and Al_2O_3—on their catalytic efficiency for CO_2 hydrogenation to methanol. The ZNC catalyst exhibits significantly better adsorption enthalpy values for H_2 and CO_2 (−6 eV and −13 eV, respectively) compared to ANC (−4 eV and −9 eV), indicating its superior capability for these molecule adsorption and activation. This superiority is further validated by H_2/CO_2-TPD experimental results, where ZNC consistently demonstrates higher uptake capacities for both hydrogen and carbon dioxide across a broad temperature range. The enhanced molecular interactions in ZNC are attributed to the strong synergy between ZrO_2 and Cu/ZnO particles, which not only facilitates hydrogen spillover but also intensifies overall catalytic activity. The increased hydrogen spillover distance in ZNC (21 Å) compared to ANC (15 Å) is a critical factor, as it enhances the mobility of reactive hydrogen species on the catalyst surface, further boosting its efficiency. The superior hydrogen spillover capacity of the ZNC catalyst is evidenced by its higher hydrogen uptake compared to the ANC catalyst, particularly in the second peak observed in the H_2-TPD profile. This enhanced spillover capability plays a pivotal role in improving the reducibility of the catalyst, as it facilitates efficient dissociation and migration of hydrogen across the catalyst surface. This, in turn, directly will contribute to ZNC's superior performance in CO_2 hydrogenation, enabling higher conversion rates and selectivity for methanol production. The underlying cause of this enhanced hydrogen spillover is rooted in the unique electronic structure of zirconia (ZrO_2), which serves as a key promoter in ZNC.

The interaction energy between Cu nanoparticles and the underlying atomic framework, along with the Metal–Support Interaction (MSI) are presented in Table 4. The superior metal–support interaction (MSI) energy of ZNC, measured at 36 eV compared to ANC's 23 eV, highlights ZrO_2's critical role in enhancing catalyst performance. ZrO_2's ability to engage in Kubas-type interactions plays a dual role in optimizing hydrogen dynamics and fortifying MSI.[50] These interactions involve electron transfer from the Zr 3d orbital to the hydrogen 1s orbital and subsequent back donation, significantly improving hydrogen adsorption, activation, and spillover processes. This robust MSI stabilizes the dispersion of Cu nanoparticles, increasing the density and availability of active catalytic sites. The enhanced MSI in ZNC directly correlates with its higher DOR% and dispersion percentage, as evidenced by H_2-TPD/O_2 titration data, leading to better distribution of active copper sites. This synergistic effect not only enhances the reducibility and catalytic efficiency of ZNC but also underscores the pivotal role of ZrO_2 in advanced catalyst design, particularly for CO_2 hydrogenation to methanol.

Further supporting these findings, the DFT analysis of the methoxy formation reaction (CO_2-θ + 5H-θ = CH_3O-θ + H_2O-θ + 3θ) reveals a more favorable reaction pathway for ZNC, with lower forward activation energy (E_f = 16 eV) and reverse activation energy (E_r = 33 eV) compared to ANC (E_f = 9 eV and E_r = 21 eV). The significant difference in overall energy change (ΔE = −17 eV for ZNC *versus* −12 eV for ANC) highlights ZNC's thermodynamic advantage, enabling a more efficient conversion of CO_2 into methanol. The reduced energy barriers in ZNC ensure a smoother and faster progression through critical reaction intermediates, ultimately contributing to its superior catalytic performance.

The intermediate reaction involving methoxy formation plays a pivotal role in the methanol production process, as this step represents a crucial juncture in the conversion of CO_2 into methanol. By employing DFT to evaluate the minimum energy pathway (MEP), this study offers critical insights into the mechanisms of intermediate stabilization and activation. The ability of ZNC to lower energy barriers and effectively stabilize key intermediates not only underscores its superior catalytic potential but also establishes it as a promising candidate for sustainable methanol synthesis.

Overall, the DFT and experimental findings collectively promise the exceptional catalytic performance of ZNC, attributed to its robust MSI, enhanced hydrogen spillover, and

Table 4 Interaction energy between Cu nanoparticles and the underlying atomic framework, along with the MSI (eV), average of H-spillover (Å), H_2 and CO_2 adsorption enthalpy (eV) of both catalysts are computed by the DFT computation

	$\Delta H_{(ads)}$ of H_2 (eV)	$\Delta H_{(ads)}$ of CO_2 (eV)	Hydrogen spillover (Å)	MSI (eV)
ZNC	−6	−13	21	36
ANC	−4	−9	15	23

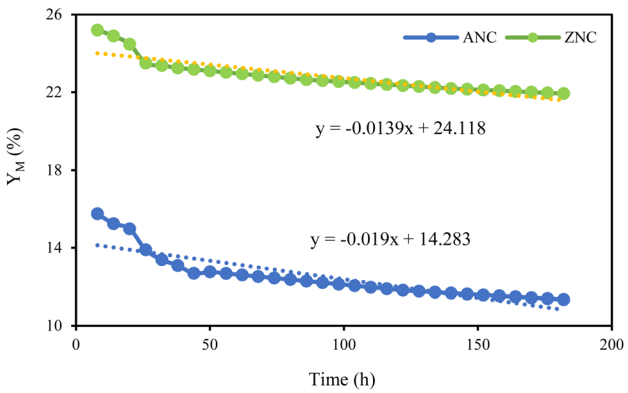

Fig. 9 Yield of methanol for both catalysts *versus* TOS of 182 hours at 150 °C, H_2/CO_2 = 3, GHSV = 4000 h^{-1}, and 30 bar.

Table 5 The catalytic test results on both catalysts were done on a 0.3 g sample at 150 °C, $H_2/CO_2 = 3$, GHSV = 4000 h^{-1}, and various pressures. X_{CO_2}%, S_M%, S_{CO}% and S_{CH_4}% respectively represent CO_2 conversion, methanol, CO, methane selectivity and P_M

	Pressure (bar)	X_{CO_2} (%)	S_M%	S_{CO}%	S_{CH_4}%	P_M (mol kg_{cat}^{-1} h^{-1})
ZNC	25	23	79	12	9	4.9
	27.5	25	83.5	9.5	7	5.8
	30	28	90	6	4	6.6
ANC	25	16	67	19	14	4.1
	27.5	18	71.5	17.5	11	4.9
	30	21	75	17	8	5.6

superior adsorption capabilities, which collectively pave the way for achieving the MEP in the CO_2 hydrogenation process.

3.3 Catalytic activity

The catalytic performance of ZNC and ANC catalysts in CO_2 hydrogenation to methanol reveals distinct differences that highlight the critical influence of the support–promoter system on their efficiency. Under identical conditions, ZNC consistently demonstrates higher CO_2 conversion (X_{CO_2}%), methanol selectivity (S_M%), and P_M, with notably lower S_{CO}% and S_{CH_4}% compared to ANC. For example, at 30 bar, ZNC achieves a CO_2 conversion of 28%, a methanol selectivity of 90%, and an P_M of 6.6 mol kg_{cat}^{-1} h^{-1}, outperforming ANC, which reaches only 21% CO_2 conversion, 75% methanol selectivity, and an P_M of 5.6 mol kg_{cat}^{-1} h^{-1}. The equilibrium CO_2 conversion at 30 bar and 150 °C, according to Jiang *et al.*,[1] is approximately 35%, indicating that our results are in reasonable compliance with equilibrium conditions. This suggests that the methanol selectivity observed for ZNC is high, as expected at these conversions, while the CO selectivity increases in ANC. Additionally, carbon and mass balances were carefully monitored and consistently exceeded 95%, confirming the accuracy of the product distribution.

This superior performance of ZNC can be attributed to several factors stemming from its structural and compositional characteristics. The ZrO_2 support in ZNC significantly enhances MSI, as evidenced by the higher MSI energy (36 eV) compared to ANC (23 eV) observed in DFT analyses. This stronger MSI stabilizes active Cu sites, improves Cu/ZnO dispersion, and facilitates the formation of oxygen vacancies, which are essential for activating and stabilizing CO_2 and hydrogen intermediates. The synergy between ZrO_2 and Cu/ZnO also promotes hydrogen spillover, as demonstrated by the H_2-TPD results, where ZNC exhibits superior hydrogen uptake at both low and high-temperature ranges compared to ANC.

In contrast, the ANC catalyst, supported by Al_2O_3, exhibits weaker MSI, reduced reducibility, and lower H_2/CO_2 adsorption capacities, which limit its catalytic activity. The XRD and BET analyses further corroborate these findings, showing that ZNC has smaller Cu particle sizes, higher dispersion, and a larger surface area than ANC catalyst, all of which contribute to enhanced catalytic efficiency.

Moreover, the CO_2-TPD results underline the role of basicity in influencing CO_2 activation, illustrate that the ZNC exhibits a higher density of medium and strong basic sites, which are closely linked to methanol synthesis, compared to ANC, which is dominated by weak basic sites. This disparity is critical, as strong basic sites, facilitated by ZrO_2, provide robust adsorption and activation of CO_2, enabling a more efficient hydrogenation pathway.

The degradation behavior over time also demonstrates the stability and durability advantage of ZNC, as illustrated in Fig. 9. Over 182 hours of time-on-stream (TOS), ZNC loses only 13% of its conversion efficiency (slope = 0.0139), whereas ANC experiences a 28% reduction (slope = 0.019). This difference further underscores the role of ZrO_2 in maintaining catalyst stability by preventing agglomeration of Cu particles and sustaining active site availability. The primary cause of deactivation is believed to be coke formation, which blocks active sites and causes particle agglomeration. ZrO_2 in ZNC helps to disperse Cu particles and reduce coke deposition, leading to enhanced catalyst stability.

In conclusion, the ZNC catalyst's superior performance in CO_2 hydrogenation to methanol can be attributed to its optimized MSI, enhanced basicity, and improved structural and textural properties. These features collectively enable higher CO_2 conversion, methanol selectivity, and long-term stability compared to the ANC catalyst. The findings underscore the importance of selecting appropriate support–promoter systems, such as ZrO_2, in designing advanced catalysts for sustainable methanol production. Future research could further optimize ZrO_2-based systems to enhance their catalytic efficiency and durability (Table 5).

4. Conclusion

The comparative analysis of ZNC and ANC catalysts highlights the critical role of metal–support interactions (MSI) in optimizing catalytic performance for CO_2 hydrogenation to methanol. ZNC, supported by ZrO_2, consistently outperforms ANC, exhibiting superior CO_2 conversion rates and methanol selectivity. This enhanced performance is attributed to the synergistic effects of ZrO_2 and the nitrogen-doped carbon layer derived from the ZIF-8 precursor. ZrO_2 plays a pivotal role by facilitating oxygen vacancy formation, enabling effective hydrogen spillover, and strengthening MSI. These properties enhance Cu nanoparticle dispersion, reducibility, and H_2/CO_2 adsorption, all of which are essential for efficient methanol synthesis.

In contrast, the ANC catalyst, supported by Al_2O_3, demonstrates several limitations. Its inert nature, lack of active oxygen

vacancies, and weaker MSI lead to poorer dispersion and reduced stabilization of key reaction intermediates. The larger CuO particle sizes and higher reduction temperatures observed in ANC reflect inefficient interactions between the copper and its support, ultimately limiting its catalytic activity and methanol yield.

Experimental findings, supported by DFT calculations, reveal that ZNC benefits from lower activation energy barriers and more favorable pathways for methoxy intermediate formation. These insights confirm ZNC's superior reducibility and catalytic activity, with Kubas-type interactions on the ZrO_2 surface further enhancing hydrogen uptake and spillover, critical factors in methanol production. The encapsulated structure of ZNC ensures uniform dispersion and accessibility of Cu/ZnO particles, amplifying its catalytic efficiency.

Overall, this study underscores the importance of advanced catalyst design, particularly the integration of ZrO_2 and nitrogen-doped carbon, in achieving high-performance catalysts for sustainable CO_2-to-methanol conversion. Future research should focus on optimizing ZrO_2-based systems to further enhance stability, scalability, and catalytic efficiency for industrial applications.

Conflicts of interest

There are no conflicts to declare.

Data availability

The authors state that the data supporting the findings of this study are included in the paper. If raw data files in a different format are required, they can be obtained from the corresponding author upon reasonable request. Source data is supplied with this paper.

References

1 X. Jiang, X. Nie, X. Guo, C. Song and J. G. Chen, Recent advances in carbon dioxide hydrogenation to methanol via heterogeneous catalysis, *Chem. Rev.*, 2020, **120**(15), 7984–8034.
2 T. A. Atsbha, T. Yoon, P. Seongho and C.-J. Lee, A review on the catalytic conversion of CO2 using H2 for synthesis of CO, methanol, and hydrocarbons, *J. CO_2 Util.*, 2021, **44**, 101413.
3 F. S. Bazghaleh, J. T. Darian, Y. Niktab and M. S. Yazd, A comprehensive thermodynamic equilibrium analysis of direct CO2 hydrogenation to light olefins product, *J. CO_2 Util.*, 2025, **102**, 103238.
4 Z. Li, *et al.*, Highly selective conversion of carbon dioxide to aromatics over tandem catalysts, *Joule*, 2019, **3**(2), 570–583.
5 X. Zhang, *et al.*, Utilization of CO2 for aromatics production over ZnO/ZrO2-ZSM-5 tandem catalyst, *J. CO_2 Util.*, 2019, **29**, 140–145.
6 B. M. Tackett, E. Gomez and J. G. Chen, Net reduction of CO2 via its thermocatalytic and electrocatalytic transformation reactions in standard and hybrid processes, *Nat. Catal.*, 2019, **2**(5), 381–386.
7 M. S. Yazd and J. T. Darian, A bifunctional catalyst for direct CO2 conversion to clean fuels: Mechanistic insights and a comprehensive kinetic model, *Fuel Process. Technol.*, 2024, **266**, 108152.
8 M. Safari, A. Haghtalab and F. A. Roghabadi, Promoting jet fuel production by utilizing a Ru-doped Co-based catalyst of Ru-Co@ C (Zd)@ Void@ CeO 2 in Fischer Tropsch synthesis, *RSC Adv.*, 2023, **13**(50), 35525–35536.
9 F. Biabangard, J. T. Darian and M. S. Yazd, Oxygenate-mediated catalysis for CO2 hydrogenation: A sustainable path to light olefins, *J. CO_2 Util.*, 2025, **98**, 103149.
10 F. Pontzen, W. Liebner, V. Gronemann, M. Rothaemel and B. Ahlers, CO2-based methanol and DME–Efficient technologies for industrial scale production, *Catal. Today*, 2011, **171**(1), 242–250.
11 M. Safari Yazd and A. Haghtalab, Kinetic modeling of the Fischer-Tropsch synthesis over the Co@ C (Zd)@ void@ CeO2 catalyst, *Chem. Eng. Commun.*, 2025, 1–16.
12 E. C. Ra, K. Y. Kim, E. H. Kim, H. Lee, K. An and J. S. Lee, Recycling carbon dioxide through catalytic hydrogenation: recent key developments and perspectives, *ACS Catal.*, 2020, **10**(19), 11318–11345.
13 R.-P. Ye, *et al.*, CO2 hydrogenation to high-value products via heterogeneous catalysis, *Nat. Commun.*, 2019, **10**(1), 5698.
14 S. De, A. Dokania, A. Ramirez and J. Gascon, Advances in the design of heterogeneous catalysts and thermocatalytic processes for CO2 utilization, *ACS Catal.*, 2020, **10**(23), 14147–14185.
15 A. Álvarez, *et al.*, Challenges in the greener production of formates/formic acid, methanol, and DME by heterogeneously catalyzed CO2 hydrogenation processes, *Chem. Rev.*, 2017, **117**(14), 9804–9838.
16 P. S. Murthy, W. Liang, Y. Jiang and J. Huang, Cu-based nanocatalysts for CO2 hydrogenation to methanol, *Energy Fuels*, 2021, **35**(10), 8558–8584.
17 M. B. Gawande, *et al.*, Cu and Cu-based nanoparticles: synthesis and applications in catalysis, *Chem. Rev.*, 2016, **116**(6), 3722–3811.
18 M. Safari and V. Nobakht, Encapsulation of Metal Nanoparticles (MNPs) as Catalyst, in *Nanocomposite Materials for Biomedical and Energy Storage Applications*, IntechOpen, 2022.
19 M. Abdellahi, Z. Aslani, N. Nazemi and S. Jabbrzare, Introducing ZrFe2O5 nanopowders for hyperthermia applications, *Chin. J. Phys.*, 2018, **56**(3), 880–885.
20 W. Wang, Z. Qu, L. Song and Q. Fu, CO2 hydrogenation to methanol over Cu/CeO2 and Cu/ZrO2 catalysts: Tuning methanol selectivity via metal-support interaction, *J. Energy Chem.*, 2020, **40**, 22–30.
21 A. Ahmad, *et al.*, Cu-doped zeolite imidazole framework (ZIF-8) for effective electrocatalytic CO2 reduction, *J. CO_2 Util.*, 2021, **48**, 101523.
22 H. Wang, *et al.*, Core–Shell-Structured Co–Z@ TiO2 Catalysts Derived from ZIF-67 for Efficient Production of C5+ Hydrocarbons in Fischer–Tropsch Synthesis, *Ind. Eng. Chem. Res.*, 2019, **58**(19), 7900–7908.

23 R. Bhardwaj, *et al.*, Integrated catalytic insights into methanol production: Sustainable framework for CO2 conversion, *J. Environ. Manage.*, 2021, **289**, 112468.
24 I. U. Din, *et al.*, Prospects for a green methanol thermo-catalytic process from CO2 by using MOFs based materials: A mini-review, *J. CO_2 Util.*, 2021, **43**, 101361.
25 T. Phongamwong, *et al.*, CO2 hydrogenation to methanol over CuO–ZnO–ZrO2–SiO2 catalysts: Effects of SiO2 contents, *Chem. Eng. J.*, 2017, **316**, 692–703.
26 A. Wang, *et al.*, Dissecting ZnOX/Cu interfacial self-encapsulation and methanol-induced strong metal-support interaction of the highly active alloyed CuZn and ZnO for methanol steam reforming, *Fuel*, 2024, **357**, 129840.
27 G. Pacchioni, From CO2 to methanol on Cu/ZnO/Al2O3 industrial catalyst. What do we know about the active phase and the reaction mechanism?, *ACS Catal.*, 2024, **14**(4), 2730–2745.
28 A. Beck, M. A. Newton, L. G. van de Water and J. A. van Bokhoven, The Enigma of Methanol Synthesis by Cu/ZnO/Al2O3-Based Catalysts, *Chem. Rev.*, 2024, **124**(8), 4543–4678.
29 M. S. Arabahmadi, R. Golhosseini, M. S. Yazd and F. Meshkani, Catalytic performance and hydrogen spillover in Cu/ZnO/Al2O3: Insights from DFT calculations on alkali and alkaline earth oxides promoters for CO2 hydrogenation, *J. CO_2 Util.*, 2025, **99**, 103162.
30 K. Li and J. G. Chen, CO2 hydrogenation to methanol over ZrO2-containing catalysts: insights into ZrO2 induced synergy, *ACS Catal.*, 2019, **9**(9), 7840–7861.
31 H. Li, L. Wang, X. Gao and F.-S. Xiao, Cu/ZnO/Al2O3 catalyst modulated by zirconia with enhanced performance in CO2 hydrogenation to methanol, *Ind. Eng. Chem. Res.*, 2022, **61**(29), 10446–10454.
32 K. Lee, *et al.*, Engineering nanoscale H supply chain to accelerate methanol synthesis on ZnZrO x, *Nat. Commun.*, 2023, **14**(1), 819.
33 M. Safari, A. Haghtalab and F. A. Roghabadi, A hollow void catalyst of Co@C(Z-d)@void@CeO2 for enhancing the performance and stability of the Fischer–Tropsch synthesis, *RSC Adv.*, 2023, **13**(33), 23223–23235, DOI: 10.1039/D3RA04884E.
34 Z. Shi, Q. Tan and D. Wu, Ternary copper-cerium-zirconium mixed metal oxide catalyst for direct CO2 hydrogenation to methanol, *Mater. Chem. Phys.*, 2018, **219**, 263–272.
35 T. Witoon, *et al.*, Enhanced activity, selectivity and stability of a CuO-ZnO-ZrO2 catalyst by adding graphene oxide for CO2 hydrogenation to methanol, *Chem. Eng. J.*, 2018, **334**, 1781–1791.
36 M. Safari, A. M. Haghighi and M. Torkian, Syngas Solubility in the Liquid Phase of the Fischer-Tropsch Synthesis, *Chem. Eng. Technol.*, 2024, **47**(3), 467–473.
37 M. Safari, J. Towfighi and M. Torkian, Simulation a Couple of Exothermic and Endothermic Syngas Processes in a Catalytic Plate Reactor, *World Chem. Eng. J.*, 2022, **6**(1), 5–16.
38 M. S. Yazd, A. Haghtalab and F. A. Roghabadi, Screening the Optimized Operating Condition for Fuel Production Through Fischer–Tropsch Synthesis with the Co@ C (Zd)@ void-SiO2@ CeO2 Catalyst, *Process. Integr. Optim. Sustain.*, 2024, 1–13.
39 M. Safari, A. Haghtalab and F. A. Roghabadi, Comprehensive kinetic modeling of the Fischer Tropsch synthesis over the Ru–Co@ C (Zd)@ void@ CeO2 catalyst based on a molecular dynamics evaluated mechanism, *Int. J. Hydrogen Energy*, 2024, **53**, 60–74.
40 Z. S. Far, J. T. Darian and M. S. Yazd, Bio-derived hierarchical nanoreactor with nitrogen-doped carbon for efficient CO2-assisted propane dehydrogenation, *Energy Convers. Manage.: X*, 2025, 101172.
41 Z. Mokhtari, J. T. Darian and M. S. Yazd, Ceria-doped UiO-66-derived carbon–zirconia supported vanadium catalysts for CO2-ODHP: Synergistic effects of MSI tuning, oxygen vacancies, and spillover behavior, *J. CO_2 Util.*, 2025, **102**, 103229.
42 Z. Mokhtari, J. T. Darian and M. S. Yazd, Mechanistic elucidation of MgO-doped VOx@ ZrO2 catalysts for enhanced CO2-assisted oxidative dehydrogenation of propane: Tuning oxygen vacancies, spillover, and redox–base properties, *Int. J. Hydrogen Energy*, 2025, **183**, 151854.
43 S. Sehar, F. Sher, S. Zhang, U. Khalid, J. Sulejmanović and E. C. Lima, Thermodynamic and kinetic study of synthesised graphene oxide-CuO nanocomposites: a way forward to fuel additive and photocatalytic potentials, *J. Mol. Liq.*, 2020, **313**, 113494.
44 M. K. Habibi, S. M. Rafiaei, A. Alhaji and M. Zare, ZnAl2O4: Ce3+ phosphors: Study of crystal structure, microstructure, photoluminescence properties and efficient adsorption of Congo red dye, *J. Mol. Struct.*, 2021, **1228**, 129769.
45 A. Abbasi, J. T. Darian, M. Pourmand and M. S. Yazd, Mechanistic insights into coke suppression and enhanced olefin selectivity in mixed metal oxide-modified SAPO-34 for high-performance methanol-to-olefins catalysis, *Chem. Eng. J. Adv.*, 2025, **22**, 100745.
46 M. J. Emami, J. T. Darian and M. S. Yazd, A Green Templated and Nitrogen-Incorporated SAPO-34 Catalyst for Enhanced MTO Performance, *Curr. Res. Green Sustainable Chem.*, 2025, 100463.
47 H. M. Khalafbadam, J. T. Darian and M. S. Yazd, Surface potential charge modulation and sequential etching strategies for optimizing SAPO-34 catalysts in the MTO process: mechanistic insights into catalytic performance, *Appl. Catal., A*, 2025, **700**, 120290.
48 M. M. Sabzehmeidani, H. Karimi and M. Ghaedi, Nanofibers based quaternary CeO2/Co3O4/Ag/Ag3PO4 S-scheme heterojunction photocatalyst with enhanced degradation of organic dyes, *Mater. Res. Bull.*, 2022, **147**, 111629.
49 C.-M. Chou, Y.-C. Chang, P.-S. Lin and F.-K. Liu, Growth of Cu-doped ZnO nanowires or ZnO-CuO nanowires on the same brass foil with high performance photocatalytic activity and stability, *Mater. Chem. Phys.*, 2017, **201**, 18–25.
50 M. S. Yazd, S. Motahari, M. R. Rahimpour, S. F. Moorjani and F. S. Bazghaleh, The support effect on the performance of a MOF-derived Co-based nano-catalyst in Fischer Tropsch synthesis, *Nanoscale*, 2024, **16**(41), 19422–19444.

51 H. M. Khalafbadam, J. T. Darian and M. S. Yazd, Nitrogen incorporation in SAPO-34: How urea etching improves catalyst lifetime and selectivity, *Fuel Process. Technol.*, 2025, **277**, 108318.
52 G. Wang, L. Chen, Y. Sun, J. Wu, M. Fu and D. Ye, Carbon dioxide hydrogenation to methanol over Cu/ZrO 2/CNTs: effect of carbon surface chemistry, *RSC Adv.*, 2015, **5**(56), 45320–45330.
53 R. Kam, C. Selomulya, R. Amal and J. Scott, The influence of La-doping on the activity and stability of Cu/ZnO catalyst for the low-temperature water–gas shift reaction, *J. Catal.*, 2010, **273**(1), 73–81.
54 R. Singh, K. Tripathi and K. K. Pant, Investigating the role of oxygen vacancies and basic site density in tuning methanol selectivity over Cu/CeO2 catalyst during CO2 hydrogenation, *Fuel*, 2021, **303**, 121289.
55 M. S. Yazd, J. T. Darian, F. S. Bazghaleh, M. Pourmand and F. S. Bazghaleh, Identifying and enhancing the spillover of crucial intermediates on the Fischer–Tropsch catalyst: A mechanistic approach, *Fuel Process. Technol.*, 2025, **273**, 108225.
56 K. Samson, *et al.*, Influence of ZrO2 structure and copper electronic state on activity of Cu/ZrO2 catalysts in methanol synthesis from CO2, *ACS Catal.*, 2014, **4**(10), 3730–3741.
57 S. Tada, *et al.*, Design of interfacial sites between Cu and amorphous ZrO2 dedicated to CO2-to-methanol hydrogenation, *ACS Catal.*, 2018, **8**(9), 7809–7819.
58 M. Safari, A. Haghtalab and F. A. Roghabadi, Tuning the strong metal support interaction of the Fischer-Tropsch synthesis silica-coated cobalt-based nano-catalyst, *Int. J. Hydrogen Energy*, 2024, **65**, 348–361.
59 M. S. Yazd and J. T. Darian, Green and more sustainable catalyst for CO and CO2 hydrogenation, *Energy Convers. Manage.: X*, 2025, 100929.
60 M. S. Yazd, A. Haghtalab and F. A. Roghabadi, Screening the footprints of water in the Fischer Tropsch synthesis over a Ru promoted Co-based catalyst supported by ceria, "a mechanistic insight", *Fuel*, 2025, **393**, 134996.
61 A. S. Shajahan, N. Kalarikkal, N. Garg, Y. Kawazo and B. Chakraborty, A quest to high-capacity hydrogen storage in zirconium decorated pentagraphene: DFT perspectives, *Int. J. Hydrogen Energy*, 2022, **47**(85), 36190–36203.
62 X.-Y. Xiao, *et al.*, Interface catalytic regulation via electron rearrangement and hydroxyl radicals triggered by oxygen vacancies and heavy metal ions, *Chem. Sci.*, 2023, **14**(11), 2960–2970.
63 T. Witoon, J. Chalorngtham, P. Dumrongbunditkul, M. Chareonpanich and J. Limtrakul, CO2 hydrogenation to methanol over Cu/ZrO2 catalysts: Effects of zirconia phases, *Chem. Eng. J.*, 2016, **293**, 327–336.